A diagrammatic formulation of the kinetic theory of fluctuations in equilibrium classical fluids. IV. The short time behavior of the memory function

ARTICLE *in* THE JOURNAL OF CHEMICAL PHYSICS · AUGUST 2004

Impact Factor: 2.95 · DOI: 10.1063/1.1764492 · Source: PubMed

2 AUTHORS, INCLUDING:

Madhav Ranganathan
Indian Institute of Technology Kanpur
12 PUBLICATIONS **32** CITATIONS

A diagrammatic formulation of the kinetic theory of fluctuations in equilibrium classical fluids. IV. The short time behavior of the memory function

Madhav Ranganathan* and Hans C. Andersen†
Department of Chemistry, Stanford University, Stanford, CA 94305
(Dated: March 3, 2004)

Using a recently developed diagrammatic formulation of the kinetic theory of fluctuations in liquids, we investigate the short time behavior of the memory function for density fluctuations in a classical atomic fluid. At short times, the memory function has a large contribution that is generated by the repulsive part of the interatomic potential. We introduce a small parameter that is a measure of the softness of the repulsive part of the potential. The diagrams in the memory function that contribute to lowest order in that small parameter are identified and summed to give an explicit expression for the dominant contribution to the memory function at short times. The result leads to a theory for fluids with continuous potentials that is similar to the Enskog theory for hard sphere fluids.

PACS numbers: 05.20.Dd, 05.20.Jj

I. INTRODUCTION

In the last two decades there has been a revival of interest in the kinetic theory of fluids because of its potential usefulness for understanding supercooled liquids and glasses. The mode coupling theory of Götze and coworkers[1–5] for slow relaxation in liquids has been widely applied to interpretation of experimental data and has stimulated many experimental studies. The mode coupling theory can be formulated as a set of assumptions about the memory function for the density autocorrelation function of a fluid without making use of any microscopic theory[2]. These assumptions can be tested by comparing the predictions of the theory with experimental data. However, a full understanding of the theory and its validity requires a microscopic understanding of the basis for the set of assumptions.

The microscopic theory on which Götze's mode coupling theory is based is a kinetic theory of Sjögren[6], which is ultimately based on the fully renormalized kinetic theory of Mazenko[7, 8]. The object of the theory is to calculate the correlation function for the fluctuations of the density of particles in single particle phase space (see below for the definition of the function), and to that end the memory function for the correlation function is studied. An important ingredient in Sjögren's theory is the separation of the memory function into a 'binary-collision part' and a 'more collective tail represented by a mode-mode coupling term'. The binary collision contribution is regarded as nonzero only for short times. The binary collision part is not evaluated from first principles in Sjögren's work. (In fact, a microscopic definition of it is not given in the theory.) Instead, a simple ansatz is made for the time dependence of the binary contribution to the memory function, and the parameters in the formula are obtained by relating them to the short time behavior of the density and current correlation functions, which are obtained from computer simulations. Such a separation of the memory function into two parts has a long history and goes back to the work of Levesque and Verlet[9]. In the work of Sjögren, the following assumptions are made: *i.* the binary collision contribution to the memory function is equal to the entire memory function at the initial time; *ii.* the same is true for the second derivative; and *iii.* the binary collision term decays to zero very quickly. The collective terms are assumed to be of $O(t^4)$ for short times and to represent the entire memory function at long times. These assumptions are the basis for an ansatz that models the collisional part of the memory function as a gaussian function of time.

The absence of a microscopic definition for the binary collision part and the consequent need to make such assumptions is troublesome in connection with the attempt to understand the properties of correlation functions and the validity of mode coupling theory in a regime in which the theory can be tested, namely simple atomic liquids at temperatures near the triple point. The properties of such fluids can easily be obtained by molecular dynamics computer simulations, and there have been numerous studies that have interpreted simulation results using Sjögren's procedure[10–14]. Under the conditions of these simulations, the vast separation of time scales that exists in supercooled liquids, between the time scale of a binary collision and the overall relaxation time, does not hold, and so uncertainties about the nature of the binary collision contribution can lead to uncertainties in the part of the memory function that is interpreted as due to mode coupling effects. The gaussian ansatz for the collisional part of the memory function has been called into question[10, 11, 13] in some of these studies.

We have recently developed a graphical formulation of the kinetic theory of atomic liquids[15–17]. It provides formally exact graphical expressions for time correlation functions of density fluctuations. Many features of the

*Current address: MADHAV: WHAT SHOULD I GIVE AS YOUR CURRENT ADDRESS?
†Electronic address: hca@stanford.edu

structure of the theory are similar to the fully renormalized kinetic theory of Mazenko[7, 8]. Unlike Mazenko's theory, however, all of the terms in the graphical theory are characterized well enough that their properties can be analyzed for the purpose of deriving approximations.

In this paper we use this graphical formulation to propose an explicit graphical definition of the part of the memory function that represents the effect of brief binary collisions. We identify these collisions as interatomic encounters that involve the repulsive part of the interatomic potential, and we introduce a small parameter that represents a measure of the softness of the repulsive part of the potential. The diagrams in the formally exact series that are of lowest order in that small parameter are identified and summed. A procedure for numerical evaluation is described. The identification of these lowest order terms with the binary collision part of the memory function is reasonable, and the sum of these terms does in fact lead to a result that decays to zero very quickly, in accordance with the third assumption above. However, contrary to a major assumption in Sjögren's analysis, the graphical result for the binary collision contribution is not equal to the total memory function at $t = 0$.

Section II presents a review of the graphical theory and its extension to multicomponent atomic fluids. Sections III, IV, and V extend the theory in preparation for the major results of the paper. Section VI discusses a class of binary collision approximations and a numerical method for their evaluation. Section VII derives the specific binary collision approximation that describes the dominant part the short time behavior of the memory function for fluids whose potential contains a very strongly repulsive part. The results and their implications are discussed in Section VIII. In a subsequent paper, this short time approximation will be applied to the dense Lennard-Jones liquid and the results will be compared with molecular dynamics computer simulation data.

II. REVIEW OF THE GRAPHICAL KINETIC THEORY

This section reviews the results of the graphical theory (see [15–17], referred to below as papers I, II, and III) that we need for this work. That work dealt solely with a one component fluids. For a discussion of self-diffusion and related dynamical properties, the analogous results for a multicomponent system are needed. The generalization of the previous results to a multicomponent system are in fact straightforward, and this is what we will present here.

A. The system of interest

The system of interest is a classical multicomponent monatomic material. The instantaneous state of the system is specified by the total number N of particles and the position $\mathbf{r}_i$, momentum $\mathbf{p}_i$, and species label s_i for each of the particles $i = 1, \ldots, N$. This collection of information will be abbreviated as $N\mathbf{r}^N\mathbf{p}^N s^N$.

The Hamiltonian is

$$H(N\mathbf{r}^N\mathbf{p}^N s^N) = \sum_{i=1}^{N} \mathbf{p}_i \cdot \mathbf{p}_i/2m(s_i) + \sum_{i<j=1}^{N} u(\mathbf{r}_i s_i \mathbf{r}_j s_j)$$

where $m(s)$ is the mass of a particle of species s and $u(\mathbf{r}s\mathbf{r}'s')$ is the energy of the interaction between a particle of species s at $\mathbf{r}$ and a particle of species s' at $\mathbf{r}'$. (We shall often omit commas between multiple arguments of a function if there is no possibility of confusion.)

If $A(N\mathbf{r}^N\mathbf{p}^N s^N)$ denotes an arbitrary function of the mechanical state of the system, then the grand canonical ensemble average of A will be denoted $\langle A \rangle$.

A function of $N\mathbf{r}^N\mathbf{p}^N s^N$ will be called a dynamical variable, and the set of all dynamical variables can be regarded as a vector space. We use Dirac's bra-ket notation for these vectors. The function denoted $A(N\mathbf{r}^N\mathbf{p}^N s^N)$ corresponds to the vector denoted $|A\rangle$. The inner product of the vectors $|B\rangle$ and $|A\rangle$ is defined as $\langle B|A\rangle \equiv \langle B^* A\rangle$.

B. Fields that describe the density and density fluctuations

The density of particles in single particle phase space is defined as

$$f(\mathbf{R}_1\mathbf{P}_1 S_1; N\mathbf{r}^N\mathbf{p}^N s^N) \equiv \sum_{i=1}^{N} \delta(\mathbf{R}_1 - \mathbf{r}_i)\delta(\mathbf{P}_1 - \mathbf{p}_i)\delta_{S_1 s_i}$$

We abbreviate $\mathbf{R}_1\mathbf{P}_1 S_1$ as 1, with similar notation for other values of the subscripts. Such a combination of variables, abbreviated as an integer, will be called a 'point variable'. We define

$$\delta(1i) = \delta(\mathbf{R}_1 - \mathbf{r}_i)\delta(\mathbf{P}_1 - \mathbf{p}_i)\delta_{S_1 s_i}$$

with a similar notation for other values of the subscripts. Then we have

$$f(1; N\mathbf{r}^N\mathbf{p}^N s^N) = \sum_{i=1}^{N} \delta(1i)$$

Note the f is a dynamical variable (i.e. a function of $N\mathbf{r}^N\mathbf{p}^N$) as well as a function of one point variable.

We define a hierarchy of multipoint densities that describe the densities of distinct particles. The first non-

trivial member of the hierarchy is f.

$$\begin{aligned}
\psi'_0 &\equiv 1 \\
\psi'_1(1) &\equiv \sum_{i=1}^{N} \delta(1i) = f(1) \\
\psi'_2(12) &= \sum_{i_1 \neq i_2 = 1}^{N} \delta(1i_1)\delta(2i_2) \\
\psi'_n(12\ldots n) &= \sum_{i_1 \neq i_2 \neq \ldots \neq i_n = 1}^{N} \delta(1i_1)\ldots\delta(ni_n)
\end{aligned}$$

These functions are dynamical variables and members of the vector space. They can also be regarded as fields that depend on arguments that specify positions in single particle phase space.

A different set of fields, obtained by taking linear combinations of these fields, is a more convenient set of dynamical variables on which to base a kinetic theory of fluctuations. We have called this new set of fields the 'fluctuation basis'[15–20]. We define the functions $\phi_n(1\ldots n)$ in the fluctuation basis by the following iterative procedure. Let $\phi_0 \equiv \psi'_0$. Let $\phi_1(1)$ be the projection of $\psi'_1(1)$ orthogonal to ϕ_0. Let $\phi_2(12)$ be the projection of $\psi'_2(12)$ perpendicular to ϕ_0 and to all ϕ_1 functions. In general $\phi_n(1\ldots n)$ is equal to the projection of ψ'_n perpendicular to all the ϕ_m functions for $m < n$. (This is a slightly different definition from the one used in III, but it leads to the same results.)

We define a set of functions that represent the inner products of the ϕ functions.

$$F_n(1\ldots n; 1'\ldots n') = \langle \phi_n(1\ldots n) | \phi_n(1'\ldots n') \rangle$$

In particular,

$$\begin{aligned}
&F_1(1;1') \\
&\quad = \rho(1)M(1)\delta(11') + \rho(1)M(1)\rho(2)M(2)(g(11')-1)
\end{aligned}$$

where $\rho(1) = \langle f(1) \rangle$ is the ensemble average density of particles of species S_1 and $g(11')$ is the usual pair correlation function. (The former depends only on its species argument and the latter depends only on its position and species arguments.)

C. Correlation functions of the fluctuation fields

The time correlation functions of the fluctuation fields are defined as

$$\begin{aligned}
&C_{nm}(1\ldots n, t; 1'\ldots m', t') \\
&\quad \equiv \langle \phi_n(1\ldots n, t)\phi_m(1'\ldots m', t') \rangle
\end{aligned}$$

where the time dependence of a dynamical variable is generated by the Liouville operator. C_{00} is unity for all times, and the C_{10} and C_{01} functions are zero for all times. The first nontrivial function in this set is $C_{11}(1,t;1',t')$, which is equal to

$$C_{11}(1,t;1',t') = \langle \delta f(1t_1)\delta f(1't'_1) \rangle \tag{1}$$

where $\delta f(1t) \equiv f(1t) - \langle f(1t) \rangle$ denotes the deviation of $f(1t)$ from its equilibrium average. This is the correlation function for density fluctuations in single particle phase space that is the object of most kinetic theories of fluctuations and that determines, for example, the coherent neutron scattering properties of the fluid.

The equations of motion for the ϕ fields are linear, as shown in Paper II, and the time correlation functions can be expressed in terms of their equal time values and a response function χ_{nm} in the following way.

$$\begin{aligned}
&C_{nm}(1\ldots n, t; 1'\ldots m', t') \\
&\quad = \frac{1}{m!} \int d1''\ldots dm''\, \chi_{nm}(1\ldots n, t; 1''\ldots m'', t') \\
&\qquad \times F_m(1''\ldots m''; 1'\ldots m')
\end{aligned}$$

The integrations are to be interpreted as

$$\int d1 \rightarrow \int_V d\mathbf{R}_1 \int d\mathbf{P}_1 \sum_{S_1}$$

The limits on the momentum integrals are from $-\infty$ to ∞ for each of the components.

D. Graphical formula for the correlation functions

A major result of paper III is the statement that the response function χ_{nm} can be expressed diagrammatically in the following way.

$\chi_{nm}(1\ldots n, t; 1'\ldots m', t') =$ the sum of all topologically different matrix diagrams with: *i.* n left roots labeled $(1,t)$, $(2,t)$, $\ldots$ (n,t); *ii.* m right roots labeled $(1',t')$, $(2',t')$, $\ldots$ (m',t'); *iii.* free points; *iv.* $\chi^{(0)}$ bonds; *v.* $Q^{(c)}$ vertices; such that: *i.* each root is attached to a $\chi^{(0)}$ bond; *ii.* each free point is attached to a $\chi^{(0)}$ bond and a $Q^{(c)}$ vertex.

Some examples of these diagrams for χ_{11} and χ_{22} are given in Figs. 1 and 2. The diagrams that appear in the dynamical theory are similar in many ways to diagrams that appear in the Mayer theory of equilibrium statistical mechanics[21–24] and in various quantum[25] and classical[26] dynamical theories.. Each point is associated with a point variable and a time. Root points, depicted as open circles, are labeled with these quantities, and a diagram is then a function of the quantities in the labels associated with the roots. Free points, depicted as closed circles, have dummy point and time variables associated with them that are to be integrated over in the calculation of the value of a diagram. $\chi^{(0)}$ bonds, depicted as thin lines with arrows pointing from right to left. A $Q^{(c)}_{nm}$ vertex is depicted as a circle with n points on the left and m points on the right.

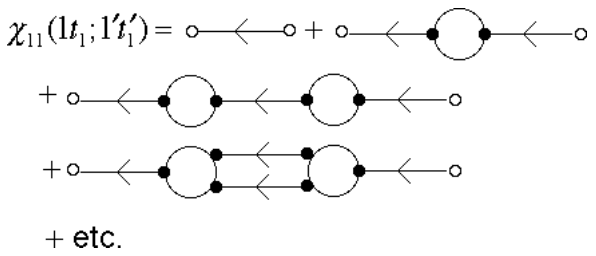

FIG. 1: The diagrammatic series for $\chi_{11}(1t_1;1't')$. In each diagram the root on the left, represented by a small open circle, should be labeled $1t_1$ and the root on the right should be labeled $1't'_1$, but the labels are omitted for simplicity. (In all the diagrams in this paper, each small open circle is a root point, each small filled circle is a free point, and each thin horizontal line with an arrow is a $\chi^{(0)}$ bond. In Figs. 1-3, each large open circle is a Q_{nm} vertex. For each such vertex, the value of n is the number of point on its left side, and the value of m is the number of points on its right side.)

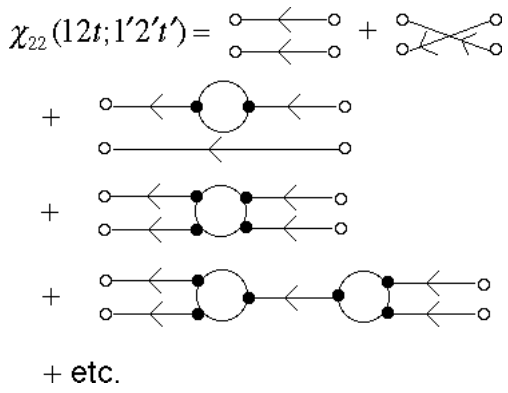

FIG. 2: The diagrammatic series for $\chi_{22}(12t;1'2't')$. Each diagram has four roots. The upper left, lower left, upper right, and lower right roots should be labeled $1t$, $2t$, $1't'_1$, and $2't'_1$, respectively. See the caption of Fig. 1 for more information. (Note that the crossing of two $\chi^{(0)}$ bonds, as in the second diagram is of no topological significance.)

Unlike the case for Mayer diagrams, the orientation of objects in the diagrams is important. There is a distinction between left roots, corresponding to left arguments of the corresponding function, which should be drawn on the far left of the diagram, and right roots, corresponding to right arguments, that should be drawn on the far right. Similarly, a $Q^{(c)}_{nm}$ vertex should be drawn so that its n left points are on the left and its m right points are on the right, and a $\chi^{(0)}$ bond should be drawn with the arrow pointing to the left. The phrase 'matrix diagram' is meant to denote the following series of restrictions: *i.* Each left root is attached to a left point of a vertex or bond and to nothing else. *ii.* Each right root is attached to the right point of a vertex or bond and to nothing else. *iii.* Each free point is attached to the right point of one vertex or bond and the left point of another vertex or bond and to nothing else.

The value of a diagram is obtained by the following procedure. 1. Assign a distinct dummy point variable to each free point. 2. Assign a distinct dummy time variable to each interaction, and assign to each free point the time variable of the interaction to which it is attached. 3. Write the product of the functions associated with each vertex and each bond. 4. Integrate over the dummy variables. 5. Divide by the symmetry number of the graph. The result is the value of the diagram.

In performing the evaluation, the following should be noted. 1. The limits on all the time integrations are $-\infty$ to ∞. 2. The symmetry number of a graph is obtained (in the usual way[22–24]) by assigning distinct labels to each of the free points and counting the number of permutations of the labels that leads to a topologically equivalent labeled graph. In determining topological equivalence for these graphs, the n left points of a $Q^{(c)}_{nm}$ vertex are equivalent to each other and the m right points are equivalent to each other, but the left and right points are topologically distinguishable from each other. 3. In these graphs, a root point is never on an interaction. In the graphical representation of some other functions, such as a memory function, a root point can be on an interaction. In that case, the time assigned to the interaction is not a dummy variable but is the same as the time attached to the root.

For example, the value of the fourth diagram in Fig. 1 is

$$\frac{1}{2}\int d3dt_3d4d5d6dt_6d7d8\,\chi^{(0)}(1,t_1;3,t_3)Q^{(c)}_{12}(3;4,5) \times\chi^{(0)}(4,t_3;6,t_6)\chi^{(0)}(5,t_3;7,t_6)Q^{(c)}_{21}(6,7;8) \times\chi^{(0)}(8,t_6;2,t'_1)$$

E. Functions appearing in the diagrams

The $\chi^{(0)}$ function is a causal propagator of the form

$$\chi^{(0)}(1t_1;1't'_1) = \Theta(t_1 - t'_1)\delta(11') \tag{2}$$

where

$$\delta(11') = \delta(\mathbf{R}_1 - \mathbf{R}'_1)\delta(\mathbf{P}_1 - \mathbf{P}'_1)\delta_{S_1S'_1}$$

To define the $Q^{(c)}$ vertices, we first define a set of functions denoted Q_{nm}.

$$\begin{aligned} &Q_{nm}(1\ldots n;1'\ldots m') \\ &\equiv \frac{1}{m!}\int d1''\ldots dm''\,W_{nm}(1\ldots n;1''\ldots m'') \\ &\quad\times K_m(1''\ldots m'';1'\ldots m') \end{aligned} \tag{3}$$

Here the W functions are matrix elements of the Liouville operator between members of the fluctuation basis:

$$\begin{aligned} &W_{nm}(1\ldots n;1'\ldots m') \\ &\equiv -\langle\phi_n(1\ldots n)|iL|\phi_m(1'\ldots m')\rangle \\ &= k_BT\langle\{\phi_n(1\ldots n),\phi_m(1'\ldots m')\}\rangle \end{aligned} \tag{4}$$

L is the Liouville operator corresponding to the Hamiltonian.

$$L = -i\sum_{i=1}^{N} \frac{\mathbf{p}_i}{m(s_i)}\cdot\nabla_{\mathbf{r}_i} + i\sum_{i<j=1}^{N} \nabla u(\mathbf{r}_i s_i \mathbf{r}_j s_j)\cdot\left(\nabla_{\mathbf{p}_i} - \nabla_{\mathbf{p}_j}\right)$$

$\{A, B\}$ denotes the Poisson bracket of A and B. The K functions are a set of matrix inverses of the F functions. They are defined so that

$$\frac{1}{n!}\int d1''\ldots dn''\, K_n(1\ldots n; 1''\ldots n'') \times F_n(1''\ldots n''; 1'\ldots n') = \mathbf{I}(1\ldots n; 1'\ldots n')$$

where

$$\mathbf{I}(1\ldots n; 1'\ldots n') = \sum_{\mathcal{P}(1'\ldots n')} \mathcal{P}\left[\delta(11')\delta(22')\ldots\delta(nn')\right]$$

Here $\mathcal{P}(1'\ldots n')$ is a permutation of the arguments $1'\ldots n'$ and the sum is over all $n!$ distinct permutations.

When $Q_{nm}(1\ldots n; 1'\ldots m')$ is analysed, it is found that this function contains some terms that have one or more factors of the form $\delta(11')$ or $\delta(12')$, i.e. a delta function connecting some left (unprimed) argument and some right (primed) argument, such that these arguments appear nowhere else in the term. When all terms with this characteristic are omitted, the remainder defines a function we denote $Q^{(c)}_{nm}(1\ldots n; 1'\ldots m')$.

We note the following: *i.* Each $Q^{(c)}$ function can be expressed in terms of the static correlation functions of the system with no direct reference to the interatomic potential. *ii.* For systems with pairwise additive potentials, there is a 'selection rule' such that $Q^{(c)}_{nm} = 0$ if $|n - m| > 1$. *iii.* $Q^{(c)}_{nm} = 0$ if $n = 0$ and/or $m = 0$. *iv.* $Q^{(c)}_{n,n+1} = 0$ for $n \geq 2$.

F. The kinetic equation for the two point density fluctuation correlation function

The graphical theory for C_{11} leads to the following kinetic equation.

$$\begin{aligned}\frac{\partial C_{11}(1, t_1; 2, 0)}{\partial t} &= \int d3\, Q^{(c)}_{11}(1;3) C_{11}(3, t_1; 2, 0) \\ &\quad + \int_0^{t_1} dt_3 \int d3\, M(1, t_1; 3, t_3) C_{11}(3, t_3; 2, 0)\end{aligned}$$

where

$$\begin{aligned}&\int d3\, Q^{(c)}_{11}(1;3) C_{11}(3, t_1; 2, 0) \\ &= -\frac{\mathbf{P}_1}{m(1)}\cdot\nabla_{\mathbf{R}_1} C_{11}(1, t_1; 2, 0) \\ &\quad + \rho(1) M_M(1) \frac{\mathbf{P}_1}{m(1)}\cdot\int d3\,\nabla c(13) C_{11}(3, t_3; 2, 0)\end{aligned}$$

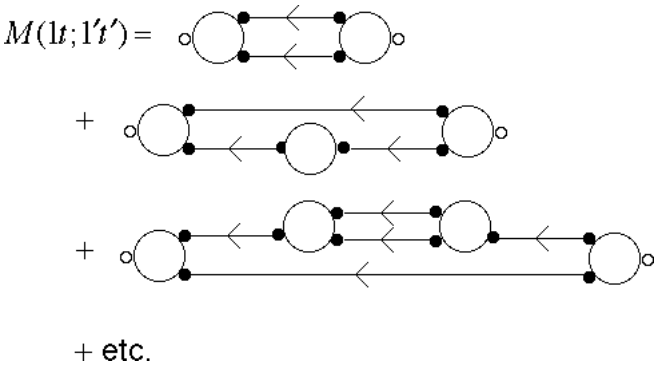

FIG. 3: The diagrammatic series for the memory function $M(1t_1; 1't'_1)$. In each diagram, the root on the left should be labeled $1t_1$ and the root on the right should be labeled $1't'_1$. See the caption of Fig. 1 for more information.

Here $M_M(1)$ is a normalized Maxwell-Boltzmann distribution function of momentum for particles of type S_1, $\rho(1)$ is the ensemble average density of particles of type S_1, and $c(13)$ is the direct correlation function for a particle of type S_1 at $\mathbf{R}_1$ and a particle of type S_3 at $\mathbf{R}_3$. Note that M_M, ρ, and c all depend on the species label in their argument. However M_M is independent of the position argument, and ρ is independent of the momentum arguments.

This equation is equivalent the usual form of the memory function equation for C_{11}[8, 27, 28]. The first term on the right of the second equality is the usual flow term. The second term is the usual Vlasov term. The third term contains the collisional part of the memory function.

The derivation of this equation leads to the following diagrammatic expression for the memory function M.

$M(1t_1; 1't'_1)$ = the sum of all topologically different matrix diagrams with: *i.* a left root labeled $(1t_1)$; *ii.* a right root labeled $(1't'_1)$; *iii.* free points; *iv.* $\chi^{(0)}$ bonds; *v.* $Q^{(c)}$ vertices; such that: *i.* the left root is attached to a $Q^{(c)}_{12}$ vertex; *ii.* the right root is attached to a $Q^{(c)}_{21}$ vertex; *iii.* each free point is attached to a $\chi^{(0)}$ bond and a $Q^{(c)}$ vertex; *iv.* there is no $\chi^{(0)}$ bond whose removal disconnects the two roots.

See Fig. 3.

G. Summary

The discussion above states some of the results of the previous three papers in this series, generalized for multicomponent systems. They can be used as the starting point for the derivation of kinetic equations and approximate theories.

See Appendix B for a discussion of the relationship of this formulation of kinetic theory and that of Mazenko.

III. PROPERTIES OF THE $Q^{(c)}_{nm}$ FUNCTIONS

The $Q^{(c)}_{nm}$ functions are the fundamental objects that generate dynamics in the graphical theory. They are defined in Eqs. (3) and are in fact rather complicated. Each can be expressed as a sum of contributions with rather different character and different physical and mathematical properties. In developing approximations using the cluster theory, it will be useful to analyze the $Q^{(c)}$ vertices into its several contributions, just as in the Mayer cluster theory it is often worthwhile to analyse the Mayer f function into various contributions from different parts of the potential. In this section, we perform such an analysis and discuss some of the properties of the various types of contributions. The basis for the analysis is the existence of delta function relationships connecting the left and right arguments of the function.

Consider the ensemble average of a ψ' function.

$$\begin{aligned}\langle\psi'_n(1\dots n)\rangle &= \left\langle \sum_{i_1\neq i_2\neq\dots i_n=1}^{N} \delta(1i_1)\dots\delta(ni_n)\right\rangle \\ &= \rho(1)M_M(1)\dots\rho(n)M_M(n)g_n(1\dots n)\end{aligned}$$

Here g_n is a multipoint static correlation function of the density in single particle position space. It is a function of only the position arguments, and it describes the correlations among n *distinct* particles. For $n = 2$, g_2 is the familiar pair correlation function denoted g. The g_n function is dimensionless, and it approaches unity when all its position arguments are well separated in space. Next consider the inner product of two ψ' functions.

$$\begin{aligned}&\langle\psi'_n(1\dots n)|\psi'_m(1'\dots m')\rangle \\ &= \left\langle \sum_{i_1\neq i_2\neq\dots i_n=1}^{N} \delta(1i_1)\dots\delta(ni_n)\right. \\ &\quad\left.\times \sum_{j_1\neq j_2\neq\dots j_m=1}^{N} \delta(1'j_1)\dots\delta(n'j_m)\right\rangle\end{aligned}$$

The terms in which all the i variables are different from all j variables involve $n+m$ distinct particles, and the sum of these terms is clearly $\langle\psi'_{n+m}(1\dots n1'\dots m')\rangle$. The terms in which, for example, $i_1 = j_1$ but all the other i variables are distinct from all the j variables, involves $n+m-1$ distinct particles and is equal to $\delta(11')\langle\psi_{n+m-1}(1\dots n2'\dots m')\rangle$. It is clear therefore that this inner product can be expressed as a sum of contributions each of which has: *i.* factors of zero or more delta functions, each of which connects one left argument with one right argument, and *ii.* a factor of a $\langle\psi\rangle$ function whose arguments are $1\dots n$ supplemented by all the primed arguments that do not appear in delta functions. None of the terms have delta function connections between left arguments, or delta function connections between right arguments, or more than one delta function connection for the same argument.

This combination of properties is shared by a number of the functions in the theory. In particular, using the methods of papers I-III, it can be shown that the $Q^{(c)}_{nm}$ functions have these properties.

We define $Q^{(c,p)}_{nm}(1\dots n;1'\dots m')$ to be the sum of all the contributions to $Q^{(c)}_{nm}(1\dots n;1'\dots m')$ that have p delta function relationships that are between the following pairs of arguments: 1 and $1'$, 2 and $2'$, …, p and p'.

The value of p can be any integer from 0 to the smaller of m and n. For example, $Q^{(c,p)}_{32}(1;1')$ is defined for $p = 0$, 1, or 2. However, in some special cases, not all values of p have nonzero functions.

The $Q^{(c,p)}_{nm}(1\dots n;1'\dots m')$ function is symmetric under the following permutations of its arguments: *i.* any permutation of $1\dots p$ provided $1'\dots p'$ are permuted in the same way; *ii.* any permutation of $p+1,\dots n$; *iii.* any permutation of $(p+1)',\dots,m'$.

The relationship between $Q^{(c)}_{nm}(1\dots n;1'\dots m')$ and $Q^{(c,p)}_{nm}(1\dots n;1'\dots m')$ is most conveniently expressed in terms of diagrams of a certain type. These diagrams have the same overall structure as the ones introduced above except there are no time arguments associated with the roots and no time component to the dummy variables. (Papers I-III make extensive use of these types of diagrams to prove relationships among the F_n, K_n, $Q^{(c)}_n$, and closely related functions.) The result is:

$Q^{(c)}_{nm}(1\dots n;1'\dots m')$ = the sum of all topologically different matrix diagrams containing: *i.* n left roots labeled $1,\dots,n$; *ii.* m right roots labeled $1',\dots,m'$; *iii.* one $Q^{(c,p)}_{nm}$ vertex.

The special symmetry of the $Q^{(c,p)}_{nm}$ function must be taken into account when determining topological equivalence of diagrams and when evaluating diagrams.

If $p > n$, the function $Q^{(c,p)}_{nm}(1\dots n;1'\dots m')$ contains a factor of $\rho(p+1)M_M(p+1)\dots\rho(n)M_M(n)$. Otherwise there are no factors of ρM_M whose arguments are the arguments of $Q^{(c,p)}_{nm}$. The function may contain factors of ρM_M for dummy integration variables, as well as factors containing static correlation functions, the direct correlation function, and multiparticle generalizations of the direct correlation function. However, there are no inverse powers of ρ. Thus, the vertices that are nonzero in the limit of zero density are those in which $p = n$.

For future reference, here are explicit formulas for some of these functions.

$$Q^{(c,1)}_{11}(1;1') = -\frac{\mathbf{P}_1}{m(1)}\cdot\nabla_R\delta(11')$$

$$Q^{(c,0)}_{11}(1;1') = \rho(1)M_M(1)\frac{\mathbf{P}_1}{m(1)}\cdot\nabla_R c(11')$$

$$Q^{(c,1)}_{12}(1;1'2') = \nabla_R u(12')\cdot\nabla_P\delta(11') \qquad (5)$$

$$Q_{12}^{(c,0)}(1;1'2') = 0$$

$$Q_{21}^{(c,1)}(12;1') = \frac{M_M(1)}{M_M(1')}\rho(2)M_M(2)g(12)\nabla_R v_{MF}(12)\cdot\nabla_P\delta(11') \tag{6}$$

$$Q_{22}^{(c,2)}(12;1'2') = (1+\mathcal{I}(12)\mathcal{I}(1'2'))\,\nabla_P\delta(11')\cdot\nabla_R v_{MF}(12)\delta(22') \tag{7}$$

Here $v_{MF}(12) \equiv -k_BT\ln g(12)$ is the potential of mean force, and $\mathcal{I}(12)$ is a permutation operator that interchanges the arguments 1 and 2 in the expression to the right. ∇_R and ∇_P, when acting on functions of two point variables, denote the gradients with regard to the first position argument and the first momentum argument, respectively. (The function W in Eq. (4) that is used for the evaluation of the Q functions in Eq. (3) can be evaluated in two ways, one involving matrix elements of the Liouville operator between ϕ functions and one involving ensemble averages of Poisson brackets of the ϕ functions. In some cases, the two methods of evaluation lead to very different looking but equivalent results. In these cases, we have given only the simpler of the two forms for each function.)

IV. THE GRAPHICAL SERIES FOR χ_{nm} IN TERMS OF $Q^{(c,p)}$ VERTICES

A. First form of the series

Substituting the graphical expression for $Q_{nm}^{(c)}$ in terms of $Q_{nm}^{(c,p)}$ into the series above for χ_{nm}, we obtain the following result:

$\chi_{nm}(1\ldots n,t;1'\ldots m',t')$ = the sum of all topologically different matrix diagrams with: *i.* n left roots labeled $(1,t)$, $(2,t)$, $\ldots$ (n,t); *ii.* m right roots labeled $(1',t')$, $(2',t')$, $\ldots$ (m',t'); *iii.* free points; *iv.* $\chi^{(0)}$ bonds; *v.* $Q^{(c,p)}$ vertices; such that: *i.* each root is attached to a $\chi^{(0)}$ bond; *ii.* each free point is attached to a $\chi^{(0)}$ bond and a $Q^{(c,p)}$ vertex.

See Fig. 4 for the diagrammatic series for χ_{11}. A $Q_{nm}^{(c,p)}$ vertex is represented as a circle with n points on the left, m points on the right, and p internal lines each of which connects a left root and a right root and indicates the presence of a δ function relationship between the corresponding pair of roots.

We also have:

$M(1t_1;1't_1')$ = the sum of all topologically different matrix diagrams with: *i.* a left root labeled $(1t_1)$; *ii.* a right root labeled $(1't_1')$; *iii.* free points; *iv.* $\chi^{(0)}$ bonds; *v.* $Q^{(c,p)}$ vertices; such that: *i.* the left root is attached to a $Q_{12}^{(c,1)}$ vertex; *ii.* the right root is attached to a $Q_{21}^{(c,p)}$ vertex; *iii.* each free point is attached to a $\chi^{(0)}$ bond and a $Q^{(c,p)}$ vertex; *iv.* there is no $\chi^{(0)}$ bond whose removal disconnects the two roots.

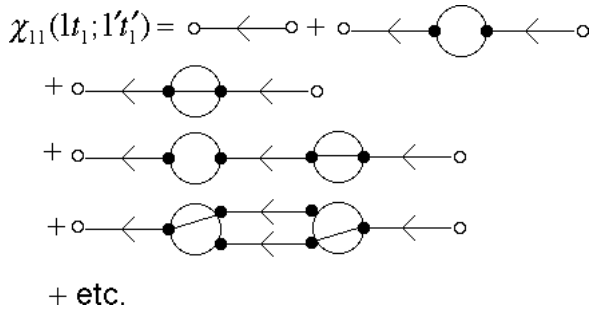

FIG. 4: The first form of the diagrammatic series for $\chi_{11}(1t_1;1't')$ in terms of $Q_{nm}^{(c,p)}$ vertices. In Figs. 4-9, each large open circle is a $Q_{nm}^{(c,p)}$ vertex, where n is the number of point on the left side, m is the number of points on the right side, and p is the number of internal lines. See the caption of Fig. 1 for more information.

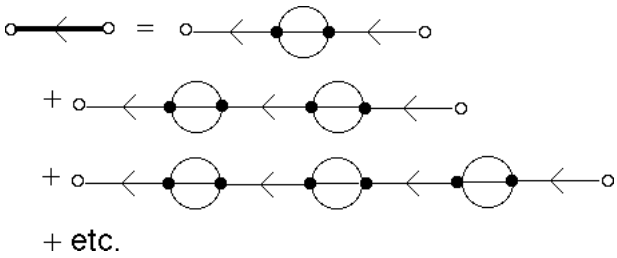

FIG. 5: Diagrammatic representation of the relationship between $\chi_{11}^{(fp)}$ and $\chi_{11}^{(0)}$. In Figs. 5-9, each thick solid line with an arrow represents a $\chi_{11}^{(fp)}$ bond. See the captions of Figs. 1 and 4 for more information.

B. Second form of the series

The $Q_{11}^{(c,1)}$ vertex is the source of the simple flow term in the kinetic equation. It generates the usual straight line, constant momentum motion of a free particle. If we were to construct the graphical theory for an ideal gas, the result for the $\chi_{11}(1t_1;1't_1')$ would be the following.

$\chi_{11}^{(fp)}(1t_1;1't_1')$ = the sum of all topologically different matrix diagrams with: *i.* one left root labeled $(1,t_1)$; *ii.* one right root labeled $(1',t')$; *iii.* free points; *iv.* $\chi^{(0)}$ bonds; *v.* $Q_{11}^{(c,1)}$ vertices; such that: *i.* each root is attached to a $\chi^{(0)}$ bond; *ii.* each free point is attached to a $\chi^{(0)}$ bond and a $Q_{11}^{(c,1)}$ vertex.

See Fig. 5 for the diagrams in this equation.

By a variety of ways it is easy to evaluate this sum, since it is the causal propagator for free particle motion.

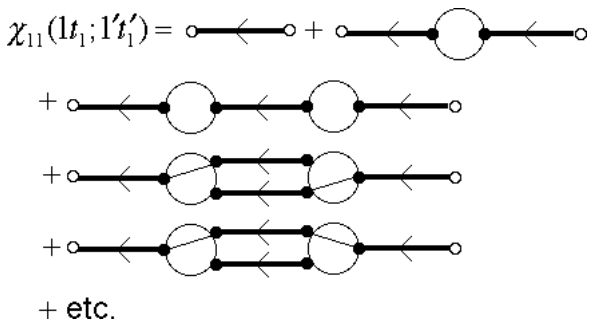

FIG. 6: The diagrammatic series for $\chi_{11}(1t_1;1't'_1)$ in terms of $\chi_{11}^{(fp)}$ bonds and $Q_{nm}^{(cp)}$ vertices. (The first and last diagrams shown here contribute to the function $\chi^{(s)}(1t_1;1't'_1)$ but the others shown here do not contribute to this function. See the text for an explanation.) See the captions of Figs. 1, 4, and 5 for more information.

The result is

$$\begin{aligned}\chi_{11}^{(fp)}&(1t_1;1't'_1)\\ &= \Theta(t_1-t'_1)\delta\left(\mathbf{R}_1-\mathbf{R}'_1-\mathbf{P}'_1(t_1-t'_1)/m(1')\right)\\ &\quad\times\delta(\mathbf{P}_1-\mathbf{P}'_1)\delta_{S_1S'_1}\end{aligned} \tag{8}$$

The diagrams in Fig. 4 (and in similar series for the general χ_{nm}) contain (among other things) $\chi^{(0)}$ bonds and $Q_{11}^{(c,1)}$ vertices. Whenever a $Q_{11}^{(c,1)}$ vertex appears, it must have a $\chi^{(0)}$ bond attached to each end. If the vertex and two bonds were removed and replaced by a single bond, the result would be valid diagram. By standard topological reduction techniques such as are used in the equilibrium theory of classical liquids (references), we can then eliminate all the $\chi^{(0)}$ bonds and $Q_{11}^{(c,1)}$ vertices in favor of $\chi_{11}^{(fp)}$ bonds. We get:

$\chi_{nm}(1\ldots n,t;1'\ldots m',t')$ = the sum of all topologically different matrix diagrams with: *i.* n left roots labeled $(1,t)$, $(2,t)$, ... (n,t); *ii.* m right roots labeled $(1',t')$, $(2',t')$, ... (m',t'); *iii.* free points; *iv.* $\chi_{11}^{(fp)}$ bonds; *v.* $Q^{(c,p)}$ vertices (but no $Q_{11}^{(1,1)}$ vertices); such that: *i.* each root is attached to a $\chi_{11}^{(fp)}$ bond; *ii.* each free point is attached to a $\chi_{11}^{(fp)}$ bond and a $Q^{(c,p)}$ vertex.

See Fig. 6.

Similarly

$M(1t_1;1't'_1)$ = the sum of all topologically different matrix diagrams with: *i.* a left root labeled $(1t_1)$; *ii.* a right root labeled $(1't'_1)$; *iii.* free points; *iv.* $\chi^{(fp)}$ bonds; *v.* $Q^{(c,p)}$ vertices (but no $Q_{11}^{(c,1)}$ vertices); such that: *i.* the left root is attached to a $Q_{12}^{(c,1)}$ vertex; *ii.* the right root is attached to a $Q_{21}^{(c,p)}$ vertex; *iii.* each free point is attached to a $\chi^{(0)}$ bond and a $Q^{(c,p)}$ vertex; *iv.* there is no $\chi^{(0)}$ bond whose removal disconnects the two roots.

See Fig. 7.

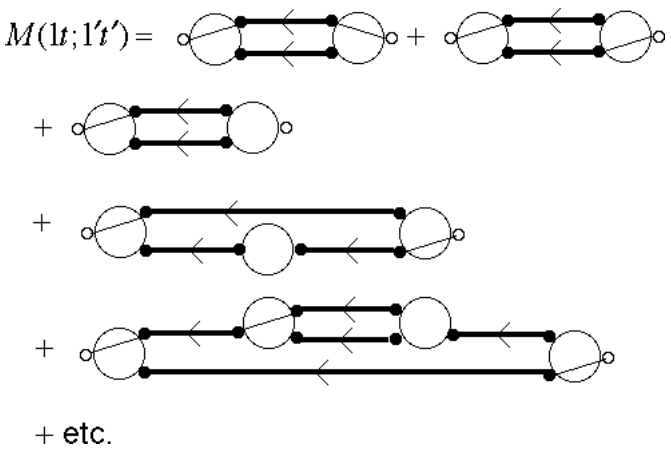

FIG. 7: The diagrammatic series for the memory function $M(1t_1;1't'_1)$ in terms of $\chi^{(fp)}$ bonds and $Q^{(c,p)}$ vertices. See the captions of Figs. 1, 4, and 5 for more information. (The first three diagrams have two particle paths. In the first two diagrams, each root is on a particle path. These diagrams are included in the binary collision approximation (BCA) as we have defined it. In the third diagram, the right root is not on one of the two particle paths, and this diagram is not included in the BCA. See the text for further discussion of the BCA.)

V. SELF CORRELATIONS

The C_{11} correlation function defined in Eq. (1) describes density fluctuations in a fluid and is related to the observable in coherent neutron scattering experiments. For an understanding of self-diffusion and incoherent neutron scattering, a different correlation function is needed. One convenient choice is the following function.

$$C^{(s)}(1t_1;1't'_1) = \frac{1}{\rho(1)}\left\langle\sum_{i=1}^{N}\delta f_i(1't_1)\delta f_i(1t'_1)\right\rangle$$

where $\delta f_i(1t_1) \equiv \delta(1i) - \langle\delta f_i(1t_1)\rangle$ is the fluctuation in the density of particle i at time t from its ensemble average. Except for the prefactor, the right side of this equation is equivalent to Eq. (1) after terms that represent correlations between different particles are removed from the latter. For $S_1 = S'_1$, this function describes self-correlations among particles of species S_1. For $S_1 = S'_1$, this function is identically zero.

$C^{(s)}$ can be calculated from the graphical theory for C_{11} in the following way. Consider adding a trace concentration of an additional species, with species label T, whose physical properties (mass, interactions) are the same as those of species S_1. It is straightforward to show that in the thermodynamic limit

$$\begin{aligned}C^{(s)}&(\mathbf{R}_1,\mathbf{P}_1,S_1,t_1;\mathbf{R}'_1,\mathbf{P}'_1,S_1,t'_1)\\ &= \lim_{\rho_T\to 0} C_{11}(\mathbf{R}_1,\mathbf{P}_1,T,t_1;\mathbf{R}'_1,\mathbf{P}'_1,T,t'_1)/\rho(T)\end{aligned}$$

where the quantity on the left side is the $C^{(s)}$ function for species S_1 for the fluid of interest and the quantity on

the right is the correlation function of the trace species in the system that contains the added trace species.

When the graphical series for the C_{11} on the right is analysed and the limit $\rho(T) \to 0$ is taken, many diagrams vanish. It can be shown that the remaining diagrams are an easily characterized (see below) subset of the diagrammatic series for $C_{11}(\mathbf{R}_1, \mathbf{P}_1, t_1; \mathbf{R}'_1, \mathbf{P}'_1, t'_1)/\rho(1)$ for the original system without the trace species. It follows that

$$C^{(s)}(1t_1; 1't'_1) = \chi^{(s)}(1t_1; 1't'_1)\rho(1')M_M(1')$$

where

$\chi^{(s)}(1t_1; 1't'_1)$ = the sum of all diagrams in the series above for $\chi_{11}(1t_1; 1't'_1)$ in which both roots are on the same particle path.

A 'particle path' in a diagram is a path along bonds and the delta function internal relations of $Q^{(c,p)}$ vertices. See Fig. 6. The basis for this result is the fact that in the diagrams in the series for $C_{11}(\mathbf{R}_1, \mathbf{P}_1, T, t_1; \mathbf{R}'_1, \mathbf{P}'_1, T, t'_1)$ every diagram with both roots on the same vertical path is $O(\rho(T))$ but every other diagram is higher order in $\rho(T)$.

Using the same graphical methods that give the kinetic equation discussed above, we can use this latest result to derive the kinetic equation for $C^{(s)}$.

$$\begin{aligned}\frac{\partial C^{(s)}(1, t_1; 2, 0)}{\partial t} &= -\frac{\mathbf{P}_1}{m(1)} \cdot \nabla_{\mathbf{R}_1} C^{(s)}(1, t_1; 2, 0) \\ &\quad + \int_0^{t_1} dt_3 \int d3\, M^{(s)}(1, t_1; 3, t_3) C^{(s)}(3, t_3; 2, 0)\end{aligned}$$

where

$M^{(s)}(1, t_1; 1', t'_1)$ = the sum of the diagrams in $M(1, t_1; 1', t'_1)$ that have a particle path extending from the right root to the left root.

VI. BINARY COLLISION APPROXIMATIONS FOR THE MEMORY FUNCTION

Various approximate kinetic equations contain as the essential physical ingredient the idea of a binary collision between two atoms. These include the Boltzmann equation, the Enskog equation, and the generalised Boltzmann-Enskog equation of Mazenko. When the memory function is calculated in such a way that it describes a single binary collision and then this memory function is used in the kinetic equation to obtain a time correlation function, the physical meaning of the approximation is that the dynamics of an atom in the fluid consists primarily of a sequence of uncorrelated binary collisions.

While such an approximation is exact at low concentrations, it is well known not to be correct at higher densities, where various collective effects induce correlations among successive collisions of an atom. However, as discussed in Sec. I an important ingredient in current kinetic theories is the idea that at least the short time behavior of the memory function is determined by binary collisions.

The graphical theory provides a language in which to define several versions of a binary collision approximation. In this section we discuss how this can be done.

A. Graphical definition of a binary collision approximation

The exact memory function M is expressed above as a sum of diagrams that have a $Q_{12}^{(c,1)}$ vertex on the left, and a $Q_{21}^{(c,p)}$ on the right. See Fig. 7. In between there are $\chi^{(fp)}$ bonds, which represent fluctuations associated with particles propagating by free particle motion, and $Q^{(c,p)}$ vertices which represent interactions among the fluctuations. (See Appendix A for a discussion of the physical interpretation of diagrams.) At all intermediate times there are at least two propagating fluctuations, since the diagram must be such that there is no single $\chi_{11}^{(fp)}$ bond whose removal would disconnect the left roots from the right roots.

It is reasonable to specify that a *binary* collision approximation should exclude diagrams in this series that have more than two fluctuations propagating at any one time. (This restriction is sufficient to exclude diagrams that contain $Q_{nm}^{(c,p)}$ vertices for $n \geq 3$ and/or $m \geq 3$.) It is also reasonable, in defining a *binary* collision approximation, to specify that the two propagating fluctuations represent the same pair of particles all the way across the diagram. In other words, in any diagram to be included, there should be two particle paths such that all the $\chi^{(fp)}$ bonds are in those paths. This implies that $Q_{11}^{(c,0)}$ vertices do not appear in the diagrams and that each of the $Q_{22}^{(c,p)}$ vertices that appears has $p = 2$.

In each of the diagrams retained, one of the two particle paths extends to the left root of the diagram, since the $Q_{12}^{(c,1)}$ vertex on the left has a delta function relationship between its left point, which is the left root, and one of its right points. Whether or not the right root of the diagram is on one of these two paths depends on whether the $Q_{21}^{(c,p)}$ on the right of the diagram has $p = 1$ or $p = 0$. See Fig. 7 for an example. If it has $p = 0$, then the two propagating particles are both distinct from the particle at the right root. In the latter case, there are clearly three particles intimately involved in the process, although only two of them are propagating. Whether or not to include these diagrams in a 'binary collision approximation' is a matter of definition, since the third particle is merely involved in the initial conditions for the dynamics of the other two and is not itself participating in the dynamics. We shall choose to exclude these diagrams in our definition of binary collision approximation.

Thus we define a binary collision approximation (BCA) for the memory function to be one that retains only those

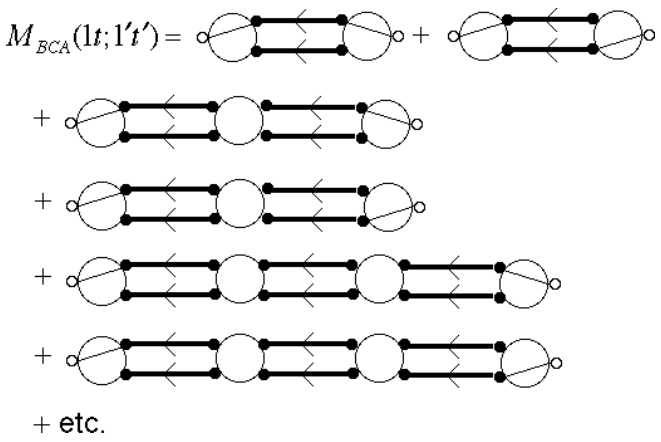

FIG. 8: The diagrammatic series for the $M_{BCA}(1t_1;1't'_1)$, the binary collision approximation for the memory function. See the captions of Figs. 1, 4, and 5 for more information.

diagrams in the memory function that have a $Q_{12}^{(c,1)}$ at the left, a $Q_{21}^{(c,1)}$ vertex on the right, $\chi^{(fp)}$ bonds, and zero or more $Q_{22}^{(c,2)}$ vertices. See Fig. 8. These diagrams have the characteristic that there are only two particle paths and each root is on one of these paths. There are two different types of diagrams: those in which both roots are on the same particle path and those in which the two roots are on different particle paths. The former type contributes to the BCA for $M^{(s)}$. Both types contribute to the BCA for M.

This binary collision approximation is closely related to, but not equivalent to, the generalized Boltzmann-Enskog approximation of Mazenko. See Appendix B for a discussion of the relationship between the two approximations.

B. Dynamical method for evaluating a binary collision approximation

The diagrams in the binary collision approximation, as we have defined it, can be evaluated by dynamical calculations involving two particles. The graphical demonstration of this result is straightforward.

We define a two particle response function that corresponds to the what lies between the $Q_{12}^{(c,1)}$ vertex on the left and the $Q_{21}^{(c,1)}$ vertex on the right in the diagrams in which both roots are on the same particle path.

$\chi_{BCA}(12t_1;1'2't'_1)$ = the sum of all topologically different matrix diagrams with: *i.* two left roots, labeled $(1,t_1)$ and $(2,t_1)$; *ii.* two right roots, labeled $(1',t'_1)$ and $(2',t'_1)$; *iii.* $Q_{22}^{(c,2)}$ vertices; *iv.* $\chi_{11}^{(fp)}$ bonds; such that: *i.* each root is attached to a $\chi^{(fp)}$ bond; *ii.* each free point is attached to a $\chi^{(fp)}$ bond and a $Q^{(c,2)}$ vertex; *iii.* there is a particle path from the right root labeled $1'$ to the left root labeled 1; *iv.* there is a particle path from the right root labeled $2'$ to the left root labeled 2.

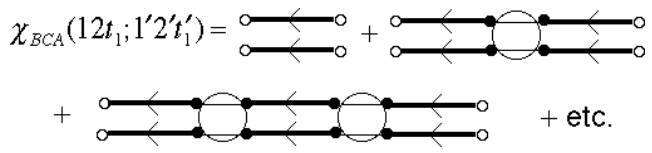

FIG. 9: Diagrammatic definition of χ_{BCA}. See the captions of Figs. 1, 4, and 5 for more information.

See Fig. 9

The binary collision approximation to the memory function in Fig. 8 can be expressed simply in terms of χ_{BCA}.

$$\begin{aligned} &M_{BCA}(1t_1;1't'_1) \\ &= \int d3d4d5d6\, Q_{12}^{(c,1)}(1;34)\chi_{BCA}(34t_1;56t'_1) \\ &\quad\times\left(Q_{21}^{(c,1)}(56;1') + Q_{21}^{(c,1)}(65;1')\right) \end{aligned} \tag{9}$$

The first term in parenthesis on the last line generates the contribution in which the two roots are on the same particle path, and the second term in parenthesis generates the contributions in which the two roots are on different paths. The binary collision approximation for the memory function for a trace species can be obtained by deleting the second term in parentheses.

To evaluate this, we derive a differential equation for the t_1 dependence of χ_{BCA}. All the t_1 dependence of each diagram in the series for this function is contained within the two $\chi_{11}^{(fp)}$ bonds attached to the two left roots. It follows from the definition of $\chi_{11}^{(fp)}$ that

$$\begin{aligned} &\frac{\partial}{\partial t_1}\chi_{11}^{(fp)}(1t_1;1''t''_1) \\ &= \int d1'''\, Q_{11}^{(c,1)}(1;1''')\chi_{11}^{(fp)}(1'''t_1;1''t''_1) \\ &\quad +\delta(t_1-t''_1)\delta(11'') \end{aligned}$$

When this is applied to the calculation of the t_1 derivative of each of the terms in the equation above for $\chi_{22,BCA}^{(>1)}$, it can be seen that the time derivative of each diagram is simply related to another diagram in the same series. A straightforward but detailed analysis yields

$$\begin{aligned} &\partial\chi_{BCA}(12t_1;1'2't'_1)/\partial t_1 \\ &= \int d1''d2''\, T(12;1''2'')\chi_{22,BCA}(1''2''t_1;1'2't'_1) \end{aligned}$$

for $t_1 > t_1'$. Here

$$\begin{aligned} T(12;1'2') \;=\; & Q_{11}^{(c,1)}(1;1')\delta(2;2') + Q_{11}^{(c,2)}(2;2')\delta(1;1') \\ & +Q_{22}^{(c,2)}(12;1'2') \end{aligned}$$

The initial condition for this differential equation is

$$\chi_{BCA}(12,t'_1+;1'2',t'_1) = \delta(11')\delta(22')$$

The differential equation can be written in a somewhat more useful form if we recognize that T can be expressed as

$$T(12;1'2') \;=\; -i\tilde{L}(12)\delta(11')\delta(22')$$

where

$$\tilde{L}(12) = L_0(1) + L_0(2) + \tilde{L}_1(12)$$

$$L_0(1) = -i\frac{\mathbf{P}_1}{m(1)}\cdot\nabla_{\mathbf{R}_1}$$

$$\tilde{L}_1(12) = i\nabla_R v_{MF}(12)\cdot(\nabla_{\mathbf{P}_1} - \nabla_{\mathbf{P}_2})$$

The operators $L_0(12)$, $\tilde{L}_1(12)$, and $\tilde{L}(12)$ are differential operators acting on functions of 12. $\tilde{L}$ is the equivalent of the Liouville operator for a two particle system whose interatomic potential is v_{MF}, which is the effective potential in $Q_{22}^{(c,2)}$. It follows that

$$\partial\chi_{BCA}(12t_1;1'2't_1')/\partial t_1 = -i\tilde{L}(12)\chi_{BCA}(12t_1;1'2't_1')$$

The solution is

$$\chi_{BCA}(12t_1;1'2't_1') = e^{-i\tilde{L}(12)(t-t_1')}\delta(11')\delta(22')\Theta(t_1-t_1')$$

When this is substituted into Eq. (9), the result can be expressed as

$$\begin{aligned} &M_{BCA}(1t;2,0)\rho(2)M_M(2) \\ &= -\int d3d4\,\rho(3)M_M(3)\rho(4)M_M(4)g(34) \\ &\quad\times\nabla_R v_{MF}(34)\cdot\nabla_{\mathbf{P}_2}\delta(3;2) \\ &\quad\times e^{i\tilde{L}(34)t}\nabla_R u(34)\cdot\nabla_{\mathbf{P}_1}(\delta(1;3)-\delta(1;4)) \end{aligned} \quad (10)$$

As is done in several kinetic theories, we introduce a basis set of functions of momentum of one particle. The basis functions will be called $H_\mu(S,\mathbf{P})$. They are labeled by an index μ. We need not specify them in detail at this point, except to say that it is convenient to choose them to be real, to be orthonormal in the following sense

$$\int d\mathbf{P}\,H_\mu(S,\mathbf{P})H_\nu(S,\mathbf{P})M_M(S,\mathbf{P}) = N_\mu\delta_{\mu\nu},$$

and to be complete in the following sense

$$\sum_\mu \frac{1}{N_\mu}H_\mu(S,\mathbf{P})H_\mu(S,\mathbf{P}')M_M(S,\mathbf{P}) = \delta(\mathbf{P}-\mathbf{P}')$$

(There are a variety of ways of constructing these functions, but it is especially convenient to use some version of Hermite polynomials because of the Gaussian nature of M_M.) In a way analogous to the notation previously used, we abbreviate $H_\mu(S_1,\mathbf{P}_1)$ as $H_\mu(1)$. We define

$$\begin{aligned} &\hat{M}_{BCA,\mu\nu}(\mathbf{k};S_1;S_2;t) \\ &\equiv \frac{1}{N_\mu N_\nu V}\int_V d\mathbf{R}_1 d\mathbf{R}_2\int d\mathbf{P}_1 d\mathbf{P}_2\, e^{-i\mathbf{k}\cdot(\mathbf{R}_1-\mathbf{R}_2)} \\ &\quad\times H_\mu(1)M_{BCA}(1,t;2,0)H_\nu(2)M_M(2) \end{aligned}$$

The $\hat{M}_{BCA,\mu\nu}$ quantities are the coefficients in a series expansion of the Fourier transform of M_{BCA} in terms of the momentum basis functions. The set of these quantities, for all values of μ and ν, as a function of t for one value of $\mathbf{k}$ are the quantities needed to calculate the Fourier transform of C_{11} for that value of $\mathbf{k}$. A straightforward evaluation using the previous results for M_{BCA}, leads to the following.

$$\begin{aligned} \hat{M}_{BCA,\mu\nu}(\mathbf{k};S_1;S_2;t) = -\frac{1}{N_\mu N_\nu}\sum_{S_4}\int d\mathbf{P}_3 d\mathbf{R}_4 d\mathbf{P}_4\, M_M(3)\rho(4)M_M(4)g(34)\nabla_R v_{MF}(34)\cdot\nabla H_\nu(3) \\ \times\nabla_R u(3(t)4(t))\cdot\left(e^{-i\mathbf{k}\cdot\mathbf{R}_3(t)}\nabla H_\mu(3(t))\delta_{S_1S_3} - e^{-i\mathbf{k}\cdot\mathbf{R}_4(t)}\nabla H_\mu(4(t))\delta_{S_1S_4}\right)\Big|_{\mathbf{R}_3=0,S_3=S_2} \end{aligned}$$

Here $3(t)$ and $4(t)$ are the phase points of two distinguishable particles at time t whose phase points at time 0 were 3 and 4. The two particles move under the influence of the potential that is in χ_{BCA}, which is v_{MF}. Note that a factor of ∇v_{MF}, derived from the $Q_{21}^{(c,1)}$ vertex, appears in this result. The $Q_{12}^{(c,1)}$ vertex generates a factor of ∇u, the force derived from the bare pair potential, and this appears as well. The corresponding result for $\hat{M}_{BCA}^{(s)}$ is obtained by deleting the second term in the parentheses in the integrand.

In the evaluation of this integrand, the initial position $\mathbf{R}_3$ of the first particle is at the origin. The integrand is nonzero for a finite range of values of $\mathbf{R}_4$, because of the ∇v_{MF} factor. The integrand can be evaluated numerically by performing trajectory calculations for two particles moving under the influence of the potential of mean force. Moreover, the integral can be evaluated by Monte Carlo methods. The Monte Carlo/trajectory calculation method for evaluating such matrix elements of

the memory function will be described in a subsequent paper.

C. Validity and usefulness of the BCA

In the limit of low density, the BCA for the memory function is exact in the sense that the memory function is of order ρ and it can be shown that all diagrams of first order in ρ are included in the BCA. Moreover, the vertices that appear in the diagrams simplify in the sense that now they can be expressed entirely in terms of the pair potential. The result is equivalent to Mazenko's low density approximation for the memory function and can be used to derive the linearized Boltzmann equation for the correlation function.

This form of the BCA should not be expected to be accurate at higher densities. The time dependence of M_{BCA} is determined by the dynamics of collisions between pairs of atoms that interact with each other via the potential of mean force and that move according to deterministic two-body classical dynamics in which the sum of the kinetic energy and the potential of mean force is conserved. It is difficult to believe that such dynamics are at all relevant for the dynamical effects in fluids that determine the long time behavior of the memory function. In the next section, we discuss a modification of the BCA that should, however, be expected to be quite accurate at short times.

VII. SHORT TIME APPROXIMATION FOR THE MEMORY FUNCTION

As noted in the introduction, the memory function for the density correlation function of atomic liquids is often regarded as the sum of one part that is large at zero time and that decays to zero rapidly and a second term that is more slowly varying and that is nonzero for long times. In this section, we use the graphical theory obtain a theoretical expression for the large short time component of the memory function M for the C_{11} correlation function. We will do this by introducing a small parameter that is a measure of the softness of the repulsive part of the potential. We investigate how the diagrams in the memory function depend on this small parameter, and we sum the diagrams that have the smallest power of that parameter.

If $u(r)$ is the interatomic potential, we define its short ranged repulsive part according to the prescription of the Weeks-Chandler-Andersen (WCA) theory of equilibrium liquids[29]:

$$\begin{aligned} u_r(r) &= u(r) - u(r_{min}) \quad \text{for } r < r_{min} \\ &= 0 \qquad\qquad\qquad\quad \text{for } r \geq r_{min} \end{aligned}$$

where r_{min} is the distance of the first minimum in the potential. The remaining part of the potential function is defined by $u_a(r) = u(r) - u_r(r)$ so that we have $u(r) = u_r(r) + u_a(r)$.

Next we choose an effective hard sphere diameter d for the repulsive part of the potential. One simple choice for d would be the distance at which the repulsive part of the potential is equal to k_BT: $u_r(d) = k_BT$. A more elaborate choice would be to use the method of the WCA theory. In either case, d is a distance that is less than r_{min}. (For the purpose of the following discussion, either of these two choices is satisfactory.)

Consider the following potential, which contains a dimensionless parameter δ.

$$u_r(r, \delta) = u_r(d + (r - d)(r_{min} - d)/\delta d)$$

The argument on the right is a scalar distance. (The argument is to be interpreted as zero if the value as written is negative.) If $\delta = (r_{min} - d)/d$, $u_r(r, d)$ is the same as $u_r(r)$, so the physically correct value of δ is $(r_{min} - d)/d$, which in many cases is small compared to unity. As $\delta \to 0$, $u_r(r, \delta)$ becomes a hard sphere potential with diameter d. Intermediate values of δ interpolate between these two limits. Thus δ is a small parameter that is a measure of the softness of the repulsive part of the potential. It is easily seen that the repulsive part of the interatomic force $-du_r(r, \delta)/dr$ is $O(\delta^{-1})$ as $\delta \to 0$.

The strategy we will adopt is to write the interatomic potential in the form

$$u(r; \delta) = u_r(r; \delta) + u_a(r)$$

and apply the graphical theory to this potential. We investigate the δ dependence of the diagrams in the series for the memory function at short times and find that there are some terms that are $O(\delta^{-1})$ for small δ. We sum all the diagrams that are of this order. The result is an approximation for the memory function that can be expected to be accurate at short times for potentials whose repulsive part is very hard as opposed to soft. Here, 'short times' means times of the order of the duration of a repulsive collision, i.e. times of $O(\delta^1)$.

If we separate the potential into two parts, u_r and u_a, the Liouville operator can be separated into terms that contain ∇u_r and terms that do not contain ∇u_r. The same separation then follows for the $Q_{nm}^{(c,p)}$ functions. (Examples of the separation are given below.) Moreover, each term that contains ∇u_r thereby has a factor that is $O(\delta^{-1})$. This is the only possible source of inverse powers of the small parameter in the evaluation of diagrams.

The presence of such an inverse power in a specific contribution to a $Q_{nm}^{(c,p)}$ vertex does not necessarily mean that the value of the function associated with the vertex is $O(\delta^{-1})$. For example, if one of the position arguments of the ∇u_r function is integrated over in the evaluation of the $Q_{nm}^{(c,p)}$ function, the integrand will be $O(\delta^{-1})$ only for a narrow range of $O(\delta)$ of positions of the integration variable. This will lead to a value for $Q_{nm}^{(c,p)}$ that is $O(\delta^0)$. Thus, the only contributions to a $Q_{nm}^{(c,p)}$ vertex that are $O(\delta^{-1})$ are those in which the ∇u_r function connects two roots of the vertex.

In sorting out all these effects, it is worthwhile to separate each $Q_{nm}^{(cp)}$ vertex into three different types of contributions. Type I contributions are those in which a ∇u_r function connects two left roots and each of those left roots is connected to a right root by a delta function relationship. Type II contributions are those in which a ∇u_r connects two roots and only one of these roots is a left root that is connected to a right root by a delta function relationship. Type I and Type II contributions are $O(\delta^{-1})$. Type III contributions are those in which either there is no ∇u_r or there is a ∇u_r but at least one of the points to which it is attached is not a root point of the $Q_{nm}^{(cp)}$ vertex. Type III contributions are $O(\delta^0)$. For some $Q_{nm}^{(cp)}$ vertices, only one or two of these parts is nonzero.

Here are some examples of the separation for the vertices that are of most important for the following discussion. A general expression for the pair correlation function of a fluid is

$$g(r) = \exp(-u(r)/k_BT)y(r)$$

where $y(r)$ is a function that is $O(\delta^0)$. Hence

$$\begin{aligned} v_{MF}(r) &= -k_BT\ln g(r) = u(r) - k_BT\ln y(r) \\ &= u_r(r) + u_a(r) - k_BT\ln y(r) \end{aligned}$$

Using Eqs. (5)-(7), we then have

$$\begin{aligned} Q_{22}^{(c,2)}(12;1'2') &= Q_{22}^{(c,2,I)}(12;1'2') + Q_{22}^{(c,2,III)}(12;1'2') \\ Q_{12}^{(c,1)}(1;1'2') &= Q_{12}^{(c,1,II)}(1;1'2') + Q_{12}^{(c,1,III)}(1;1'2') \\ Q_{21}^{(c,1)}(12;1') &= Q_{21}^{(c,1,II)}(12;1') + Q_{21}^{(c,1,III)}(12;1') \end{aligned}$$

where

$$\begin{aligned} &Q_{22}^{(c,2,I)}(12;1'2') \\ &= (1+\mathcal{I}(12)\mathcal{I}(1'2'))\,\nabla_P\delta(11')\cdot\nabla_R u_r(12)\delta(22') \end{aligned}$$

$$\begin{aligned} Q_{12}^{(c,1,II)}(1;1'2') &= \nabla_R u_r(12')\cdot\nabla_P\delta(1;1') \\ Q_{21}^{(c,1,II)}(12;1') &= \nabla_R u_r(12')\cdot\nabla_P\delta(1;1') \end{aligned}$$

Note that in each of these cases, one of the three types of contributions is zero. In addition, we note that it can be shown that $Q_{11}^{(c,p,I)} = 0$ for any p, and $Q_{n,n-1}^{(c,p,I)} = 0$ for any n and p.

Consider

$$\int d\mathbf{R}_1\, e^{i\mathbf{k}\cdot(\mathbf{R}_1-\mathbf{R}_2)} \int_0^{t_1} dt_3 \int d3\, M(1,t_1;3,t_3) \times C_{11}(3,t_3;2,0) \quad (11)$$

which is the memory function contribution to the time derivative of the spatial Fourier transform of the correlation function. More specifically, we focus on the integrand for the time integral.

$$\int d\mathbf{R}_1\, e^{i\mathbf{k}\cdot(\mathbf{R}_1-\mathbf{R}_2)} \int d3\, M(1,t_1;3,t_3) C_{11}(3,t_3;2,0) \quad (12)$$

The graphical series for M is to be substituted into this integral. Then each vertex is expressed in terms of its Types I, II, and III contributions. We obtain a series in which each vertex that appears is either Type I, II, or III. We are interested in the behavior of the various contributions for small values of t_1, i.e. $t_1 = O(\delta)$.

The order of magnitude of a contribution is of the form $O(\delta^{-n_I-n_{II}+(n_v-2)+n_\delta})$, where: n_I is the number of type I vertices, n_{II} is the number of Type II vertices, n_v is the number of vertices, and n_δ is the number of integrations whose integrands are nonzero over only a narrow range δ of the integration variable. Note that $n_v - 2$ is the number of independent time integrations that appear in the evaluation of the integral (one integration for each vertex other than the $Q_{12}^{(c,p)}$ at the left of the M and the $Q_{21}^{(c,p)}$ at the right), and each such integration leads to a factor of δ since the integrand for each time integration is nonzero only over a time range of $O(\delta)$.

If either n_I or n_{II} is nonzero, then the integration over the point at either end of any of the ∇u_r functions is restricted to a narrow range of $O(\delta)$, and hence $n_\delta \geq 1$. It follows immediately that the largest possible order of magnitude is $O(\delta^{-1})$. This can be achieved for contributions in which all vertices are type I or II and $n_\delta = 1$.

We define the short time approximation to the memory function as the sum of all the terms in the diagrammatic series for the memory function that generate a contribution of $O(\delta^{-1})$ to (12), the time integrand of (11), for times of the order of δ and that hence generate a contribution of (δ^0) to the time derivative of C_{11} for that same time range.

We can obtain a more specific and much simpler characterization of the set of diagrams that contribute to the short time approximation. The outline of the argument is the following. We are considering the entire class of diagrams that contributes to the memory function and ask which of these have the characteristics that: *i.* all vertices are type I or type II; and *ii.* $n_\delta = 1$. First, it can be shown that any diagram with a $Q_{n,n-1}^{(c,p,II)}$ vertex has $n_\delta \geq 2$. We noted above that $Q_{n,n-1}^{(c,p,I)} = 0$. It follows that the only nonzero diagrams that remain in the short time approximation are those in which the number of propagators suffers no net change between the $Q_{21}^{(c,1,II)}$ on the right and the $Q_{12}^{(c,1,II)}$ on the left. It can then be shown that of the remaining diagrams, any that has a type II vertex other than the one on the left and the one on the right has $n_\delta > 1$.

Thus, the only contributions to (1) that can possibly be in the short time approximation are those whose only vertices are a $Q_{12}^{(c,1,II)}$ vertex on the left, a $Q_{21}^{(c,1,II)}$ on the right, and a series of zero or more $Q_{22}^{(c,2,I)}$ vertices in between. A straightforward argument shows that each of these contributions has $n_\delta = 1$, and hence these contributions are indeed of $O(\delta^{-1})$.

Thus the diagrams in the memory function that contribute to the short time approximation are those in

which the vertex at the left is a $Q_{12}^{(c,1,II)}$ vertex, the one on the right is a $Q_{21}^{(c,1,II)}$ vertex, and all the other vertices that appear are $Q_{22}^{(c,2,I)}$ vertices. These are precisely the types of diagrams included in a BCA for which the repulsive part of the potential, rather than the full potential or the potential of mean force is used to evaluate the vertices. Thus, these diagrams can be summed by trajectory calculations as discussed above. We get, using 'STA' to denote the short time approximation,

$$\hat{M}_{STA,\mu\nu}(\mathbf{k};S_1;S_2;t) = -\frac{1}{N_\mu N_\nu}\sum_{S_4}\int d\mathbf{P}_3 d\mathbf{R}_4 d\mathbf{P}_4\, M_M(3)\rho(4)M_M(4)g(34)\nabla u_r(34)\cdot\nabla H_\nu(3)$$
$$\times\nabla u_r(3(t)4(t))\cdot\Big(e^{-i\mathbf{k}\cdot\mathbf{R}_3(t)}\nabla H_\mu(3(t))\delta_{S_1S_3} - e^{-i\mathbf{k}\cdot\mathbf{R}_4(t)}\nabla H_\mu(4(t))\delta_{S_1S_4}\Big)\Big|_{\mathbf{R}_3=0,S_3=S_2} \tag{13}$$

Here $3(t)$ and $4(t)$ are the phase points of two distinguishable particles at time t whose phase points at time 0 were 3 and 4. The two particles move under the influence of u_r, the repulsive part of the bare potential. $\hat{M}_{STA}^{(s)}$ can be obtained from this result by deleting the second term in parentheses.

Note that this result has the characteristic that it goes to zero for times larger than the duration of a *repulsive collision*, which is approximately equal to $r_{min} - d$ divided by the mean thermal velocity of particles. This follows because the only trajectories that contribute to this result are those that start at time 0 in a configuration in which $\nabla v_r \neq 0$, evolve in time under the influence of the repulsive part of the potential, and that at time t_1 still have $\nabla v_r \neq 0$.

In the limit of $\delta \to 0$, this is equivalent to the low density form of the memory function for the system with repulsive forces only, except for an additional factor of $g(d)$. Thus the result for nonzero δ is, in effect, a generalization of the Enskog theory that is applicable to continuous potentials. It is important to note, however, that the derivation implies that (13) is the correct short time result for the system with the complete original interatomic potential, i.e. the potential that includes both attractive and continuous repulsive parts.

VIII. DISCUSSION

The major result of this paper is Eq. (13), which is the short time approximation (STA) for the memory function in the equation for the phase space density autocorrelation function of an atomic fluid. It was derived by defining a small parameter δ that is a measure of the softness of the short range repulsive forces generated by the potential and by summing all terms in a formally exact graphical series for the memory function that are $O(\delta^{-1})$ for times of $O(\delta)$. The resulting 'short time approximation' in fact goes to zero for times much larger than $O(\delta)$. The approximation was derived for an atomic fluid whose potential has a short ranged repulsive part as well as a longer ranged attractive and/or repulsive part.

The approximation becomes a formally exact description of the short time behavior in the limit $\delta \to 0$, which corresponds to the hard sphere limit for the repulsive forces, but it will be primarily useful as an approximation for fluids with continuous repulsive potentials such as the Lennard-Jones potential and potentials commonly used for the noble gases and liquid metals. The derivation of the result gives no quantitative prediction about how 'hard' the repulsive part of the force must be in order for the approximation to be accurate at short times.

In the next paper in this series, we apply this approximation to a dense Lennard-Jones fluid and compare the predictions of the approximation with molecular dynamics computer simulations results.

The STA provides a reasonable microscopic definition of the 'binary-collision part' of the memory function (of the phase space density autocorrelation function) that is often invoked in kinetic theories of dense liquids[6, 10–13], at least for strongly repulsive potentials. To our knowledge, this is the first such microscopic definition for fluids with continuous interatomic potentials. In this connection, it is significant to note that some of the assumptions ordinarily made in estimating the binary collision contribution are not consistent with this microscopic definition. The short time approximation for the memory function, as we have defined it, is not equal to the entire memory function for $t = 0$. For example, the diagrams in the memory function that have just two vertices, a $Q_{12}^{(c,1,III)}$ on the left and a $Q_{21}^{(c,1,III)}$ on the right, are in general nonzero and of $O(\delta^0)$ at zero time. These vertices describe interactions that arise from the attractive part of the potential and of the potential of mean force. They are not included in the short time approximation, and there is no basis for thinking that they are part of a contribution that goes to zero for times much larger than δ^{-1}. Thus, the usual empirical procedure of separating the memory function into a 'binary collision part' and a 'more collective tail' that is zero at $t = 0$, which is the basis for much analysis of simulation data, still lacks a fundamental microscopic basis.

Acknowledgments

This work was supported by the National Science Foundation through grants CHE-9734893 and CHE-0010117.

APPENDIX A: PHYSICAL INTERPRETATION OF THE DIAGRAMS

Each of the diagrams in the series for the correlation functions C_{nm}, the response functions χ_{nm}, $\chi^{(0)}$, $\chi^{(fp)}$, and $\chi_{22}^{(>1)}$, and the memory function M can be given a physical meaning. This physical meaning is merely an after-the-fact interpretation and is not required for the formal development of the theory. However, a physical interpretation is very useful for the formulation of diagrammatic approximations. In this appendix, we discuss how to assign physical meaning to individual diagrams, focussing on the various response functions χ.

The $\chi_{nm}(1\dots n,t;1'\dots m',t')$ function has two time arguments (a left time argument and a right time argument) and two sets of phase space arguments (a left set and a right set). In any of the diagrams for a χ function, each open circle at the right is labeled with a phase space argument from the right set (e.g. $1'$, representing a point in single particle phase space $\mathbf{R}_1', \mathbf{P}_1'$) and the right time argument (e.g. t'). Such an open circle represents a fluctuation in the density in single particle phase space at $\mathbf{R}_1', \mathbf{P}_1'$ at time t'. Similarly an open circle at the left is always labeled with a phase space argument from the left set and with the left time argument (e.g. t). It represents a fluctuation in single particle phase space at time t. The total function χ_{nm} represents how m fluctuations at time t' propagate forward in time and generate n fluctuations at time t. Each of these functions is causal and is zero for $t < t'$.

Each diagram in the series for χ_{nm} can be regarded as one contribution to the forward propagation of these fluctuations. Each of these contributions is also causal. (Note that in these diagrams, time increases from right to left; more precisely, when a diagram is nonzero, the time at the left is after the time at the right.)

The $\chi^{(0)}$ function defined in Eq. 2 is exactly equal to χ_{11} for a system of particles that do not move. Any fluctuation at the right time still exists at the left time, provided the left time is later than the right time. Thus a thin solid line, with an arrow, represents a fluctuation that is propagating forward in time with no change.

The Q_{nm} function represent an instantaneous interaction in which m fluctuations at their respective points in single particle phase space interact to form n fluctuations at their respective points. (Any of the original m fluctuations that do to appear among the n are destroyed in this process.)

The meanings of the various diagrams in Fig. 1 can now be discussed. $\chi_{11}(1t_1;2't_1')$ represents a fluctuation that starts at $1'$ (an abbreviation for $\mathbf{R}_1'\mathbf{P}_1'$) at time t_1' and propagates to 1 at time t. The first diagram on the right represents the contribution to this that arises if there are no dynamics in the system. Its value is nonzero only if the two fluctuations are at the same point. In the second diagram, the original fluctuation, represented by the line on the right, propagates forward without change, then undergoes an interaction that yields a single fluctuation, represented by the line on the left. That new interaction propagates forward without change. In the fourth diagram on the right. A single fluctuation at the left propagates without change, undergoes an interaction that produces two fluctuations that then propagate without change. The two fluctuations then undergo an interaction that produces one fluctuation, which then propagates without change.

When these diagrams are evaluated, there is a single time variable (a dummy variable of integration) that is assigned to each interaction and to all points (closed circles) on that interaction. That time can be interpreted as the time at which the interaction takes place, and the time integration takes into account all the times at which it can take place. Because of the Heaviside functions in the $\chi^{(0)}$ functions, the integrand is nonzero only when that time satisfies certain restrictions. E.g. in the second diagram on the right, the interaction has a nonzero effect only if it takes place after time t' and before time t. In the fourth diagram on the right, the time associated with the right interaction must be earlier than the time associated with the left interaction (and both must be between t_1' and t) in order for the contribution to be nonzero.

If we assign times to each of the interactions in a diagram in such a way that the integrand in the value of the diagram is nonzero, then we can make statements about the number of fluctuations that are propagating in each time interval. For example, in the evaluation of the fourth diagram on the right of Fig. 1 in 2, we assigned time t_6 to the right interaction and t_3 to the left interaction. The integrand is nonzero only for $t_1 > t_3 > t_6 > t_1'$. It is clear that one fluctuation propagates in the time interval between t_1' and t_6, two fluctuations propagate between t_6 and t_3, and one fluctuation propagates between t_3 and t. Statements about the numbers of fluctuations propagating in intervals play a useful role in discussing the various functions and in motivating various approximations. For example, a characteristic of the function $\chi_{22}^{(>1)}$, which is closely related to the memory function, is that its diagrams have no $\chi^{(0)}$ bond whose removal disconnects both left roots from both right roots. This is equivalent to the statement that there is no time interval in which only one fluctuation is propagating. In other words, in the $\chi_{22}^{(>1)}$ diagrams, every time interval has at least two propagating fluctuations.

The previous physical interpretation of diagrams in terms of the propagation and interaction of fluctuations is appropriate for diagrams that contain $Q^{(c)}$ vertices. Diagrams that contain $Q^{(c,p)}$ vertices can be interpreted in a slightly different way in terms of fluctuations that

are identified with particles.

A fluctuation in density at a point in single particle phase space can be regarded as caused by the presence or absence of a specific particle at that point. In $\chi^{(0)}$, which is represented by a thin line with an arrow, the fluctuation at the right and the fluctuation at the left correspond to the same particle, which is not moving. In the $Q^{(c)}_{nm}$ vertices, there is in general no relationship between the particles corresponding to the fluctuations on the left and the particles corresponding to the fluctuations on the right. In the $Q^{(c,p)}_{nm}$ vertices, however, there is such a relationship. For such a vertex, there are $n+m-p$ distinct particles corresponding to the fluctuations in the n left points and m right points. p of these particles are associated with fluctuations that are both on the left and the right. An internal line in the vertex connects a point on the right and a point on the left that are associated with the same particle. $m-p$ of these particles are associated only with points or fluctuations on the right. $n-p$ of these particles are associated only with points or fluctuations on the left.

For diagrams containing $Q^{(c,p)}$ vertices (rather than $Q^{(c)}$ vertices), a particle path is defined as a connected path along bonds and internal lines of the $Q^{(c,p)}$ vertices. Such a path represents a single particle participating in the fluctuation history described by the diagram. Any two particle paths that intersect the same $Q^{(c,p)}$ vertex clearly represent two distinct particles.

A $\chi^{(fp)}_{11}$ bond (see Eq. 8) represents the exact χ_{11} for an ideal gas of particles whose Hamiltonian contains only kinetic energy. From its graphical representation (see Fig. 5), it can be seen that it represents all possible particle paths that go from the right root to the left root along a series of one or more $\chi^{(0)}$ bonds and zero or more $Q^{(c,1)}_{11}$ vertices. It represents propagation of a fluctuation due to a single particle moving in space with constant momentum.

Fig. 6 gives the diagrammatic representation of χ_{11}. The first diagram on the right side of the equation represents a fluctuation that corresponds to a single particle moving freely from the right root to the left root. In the second diagram, a fluctuation at the right root corresponds to a particle that moves freely for some time and then undergoes an interaction that creates a fluctuation involving a second particle and that destroys the original fluctuation. The second particle propagates freely to the left root. In the fourth diagram, the particle at the right corresponds to a particle that moves freely for some time, undergoes an interaction that creates a fluctuation due to a distinct particle, while preserving the fluctuation due to the original particle. The two particles propagate freely and interact once again. The second particle then propagates freely to the left root.

APPENDIX B: RELATIONSHIP OF THE GRAPHICAL THEORY TO THE FULLY RENORMALIZED KINETIC THEORY OF MAZENKO

The structure of the results of the graphical kinetic theory presented here is similar to those of the fully renormalized kinetic theory of Mazenko[7, 8], despite the very different types of formal manipulations used in the two theories. In this appendix, we comment on the relationship between the two theories, in terms of the nature of the theoretical techniques used and a comparison of specific results of the two theories.

The graphical theory presented here is based on the use of a projection operator method to construct the fluctuation basis and diagrammatic methods to analyze the equations of motion for the fluctuation fields. Mazenko's method does not use projection operators; instead it uses algebraic techniques to derive a formal expression for the memory function. Mazenko's method does not make explicit use of diagrammatic techniques, but some of the language used in the presentation of the results ('connected' and 'disconnected' functions, 'endpoint vertices') appears to be inspired by diagrammatic formalisms. Mazenko's theory has the formal structure of a hierarchy of correlation functions and memory functions involving larger and larger numbers arguments and a set of formal relationships between members of the hierarchy. The successive terms in the hierarchy appear to correspond to the introduction of the successive basis functions of the fluctuation basis. In particular, this is clearly true up to and including the ϕ_2 basis functions. Many of the important functions defined in Mazenko's theory can be interpreted as matrix elements of various operators among the first two nontrivial basis functions $|\phi_1(1)\rangle$ and $|\phi_2(12)\rangle$. The amount of detail and analysis that has been presented for the subsequent levels of the hierarchy in Mazenko's theory is insufficient to decide whether the parallels to the graphical theory continues further down the hierarchy. We strongly suspect, however, that at least for problems describable by a Hamiltonian with pairwise additive interatomic potentials, the successive levels of Mazenko's hierarchy correspond precisely to the introduction of those parts of the Hilbert space of dynamical variables that are spanned by the succession of fluctuation basis functions.

We shall now state a number of miscellaneous relationships between the important quantities in Mazenko's theory and the graphical theory. *i.* The function we have called $M(1,t_1;2,t_1)$ corresponds to the negative of Mazenko's $\phi^{(c)}$, the collisional part of the memory function. *ii.* Mazenko's $\mathcal{V}$, which is referred to as an 'endpoint' vertex, corresponds, except for a numerical factor, to W_{12} and W_{21} in the graphical theory. *iii.* Mazenko's W corresponds, except for a numerical factor, to W_{22} in the graphical theory. *iv.* Mazenko's $\tilde{C}^{-1}$ function corresponds to K_1 in the graphical theory. *v.* Mazenko's $\tilde{G}^{-1}$ corresponds to K_2 in the graphical theory.

There is an important difference between the way that Mazenko chose to organize the terms in his theory to make approximations and the way that we carry out the same type of process. The fundamental dynamical vertices in our theory are the Q_{nm} vertices, analysis of which leads to identification of a part of each Q_{nm} as $Q^{(c)}_{nm}$, subsequent analysis of which leads to the definition of the $Q^{(c,p)}_{nm}$ functions on the basis of the delta function relationships that exist among the left and right roots. Each Q_{nm} vertex is derived from W_{nm} and K_m. In Mazenko's theory, the quantities analogous to W_{nm} and K_n, for $n = 0$ and 1, are analyzed separately on the basis of the same considerations. If no approximations are made, both procedures lead to equivalent correct results. However, the two procedures can suggest different approximations.

An important example of this is that in developing a binary collision approximation, Mazenko kept one part of the $\mathcal{V}$ function, the part denoted $\mathcal{V}_1$, and did not include another part $\mathcal{V}_2$. The latter can be expressed in terms of three particle correlation functions and thereby appears to be inappropriate for inclusion in a binary collision approximation. However, if the two terms are kept together as W_{12} and are combined with K_2 to construct $Q^{(c)}_{12}$, which is then analyzed, it is found that the resulting $Q^{(c)}_{12}$ is very simple and involves only two body interactions. The entire $Q^{(c)}_{12}$ vertex is retained in the binary collision approximation discussed in the text of this paper. This accounts for the fact that in our Eq. (10) the first interaction factor contains the gradient of the pair potential, whereas the corresponding expression in Mazenko's theory for a binary collision approximation contains the gradient of the potential of mean force.

[1] W. Götze and L. Sjögren, Transport Theory and Stat. Phys **24**, 801 (1995).
[2] W. Götze, in *Liquids, Freezing, and the Glass Transition*, edited by J. P. Hansen, D. Levesque, and J. Zinn-Justin (North-Holland, 1991), p. 287.
[3] W. Götze and L. Sjögren, Z. Physik B - Cond. Matter **65**, 415 (1987).
[4] W. Götze and L. Sjögren, J. Phys. C: Solid State Physics **21**, 3407 (1988).
[5] W. Götze and L. Sjögren, Rep. Progr. Phys. **55**, 241 (1992).
[6] L. Sjögren, Phys. Rev. **22**, 2866 (1980).
[7] G. F. Mazenko, Phys. Rev. **A9**, 360 (1974).
[8] G. F. Mazenko and S. Yip, in *Statistical Mechanics - Part B: Time-Dependent Processes*, edited by B. J. Berne (Plenum, 1977), p. 181.
[9] D. Levesque and L. Verlet, Phys. Rev. **2**, 2514 (1970).
[10] W. Gudowski, M. Dzugutov, and K.-E. Larsson, Phys. Rev. **E47**, 1693 (1993).
[11] M. M. G. Alemany, J. Casas, C. Rey, L. E. Gonzalez, and L. J. Gallego, Phys. Rev. **E56**, 6818 (1997).
[12] J. Casas, D. J. Gonzalez, and L. E. Gonzalez, Phys. Rev. **B60**, 10094 (1999).
[13] J. Casas, D. J. Gonzalez, L. E. Gonzalez, M. M. G. Alemany, and L. J. Gallego, Phys. Rev. **B62**, 12095 (2000).
[14] U. Balucani and M. Zoppi, *Dynamics of the Liquid State* (Oxford University Press, 1994).
[15] H. C. Andersen, J. Phys. Chem. B **106**, 106 (2002).
[16] H. C. Andersen, J. Phys. Chem. B **107**, 10226 (2003).
[17] H. C. Andersen, J. Phys. Chem. B **107**, 10234 (2003).
[18] S. J. Pitts and H. C. Andersen, J. Chem. Phys. **114**, 1101 (2001).
[19] C. D. Boley, Phys. Rev. **A11**, 328 (1975).
[20] M. Lindenfeld, Phys. Rev. **A15**, 1801 (1977).
[21] J. E. Mayer, *Statistical Mechanics* (Wiley, 1940).
[22] T. Morita and K. Hiroike, Prog. Theor. Phys. **25**, 537 (1961).
[23] G. Stell, in *The Equilibrium Theory of Classical Fluids*, edited by H. L. Frisch and J. L. Lebowitz (Benjamin, 1964), pp. II–171.
[24] H. C. Andersen, in *Statistical Mechanics Part A: Equilibrium Techniques*, edited by B. J. Berne (Plenum, 1977), p. 1.
[25] A. L. Fetter and J. D. Walecka, *Quantum theory of many-particle systems* (McGraw-Hill, 1971).
[26] H. C. Andersen, J. Math. Phys. **41**, 1979 (2000).
[27] J. P. Boon and S. Yip, *Molecular Hydrodynamics* (McGraw-Hill, 1980).
[28] J. P. Hansen and I. R. McDonald, *Theory of simple liquids* (Academic Press, 1990).
[29] J. D. Weeks, D. Chandler, and H. C. Andersen, J. Chem. Phys. **54**, 5237 (1971).